ISSN 1070-3284, Russian Journal of Coordination Chemistry, 2020, Vol. 46, No. 4, pp. 283–289. © Pleiades Publishing, Ltd., 2020.

Imidazole Multi-Carboxylate-Based 2D Cd(II) MOF: Preparation, Crystal Structure, and Properties

Y. Zhao[a], D. D. Zhao[a], H. L. Liu[a], W. Y. Zhou[b], and G. Li[b, *]

[a]*School of Chemical Engineering, Henan Technical Institute, Zhengzhou, Henan, 450042 P.R. China*

[b]*College of Chemistry and Molecular Engineering, Zhengzhou University, Zhengzhou, Henan, 450001 P.R. China*

**e-mail: gangli@zzu.edu.cn*

Received October 29, 2018; revised September 22, 2019; accepted October 10, 2019

Abstract—By adopting one imidazole multi-carboxylate ligand, 2-(3-carboxylphenyl)-1*H*-imidazole-4,5-dicarboxylic acid (*m*-$CPhH_4IDC$) and one N-containg ligand, 2,2'-bipyridine (2,2'-Bipy) to react with $Cd(NO_3)_2$, under solvothermal condition, a two-dimensional metal-organic framework, $\{[Cd_6(m\text{-}CPhHIDC)_4(2,2'\text{-}Bipy)_6] \cdot 4H_2O\}_n$ (**I**) has been sucessfully constructed. The structure has been determined by single-crystal X-ray diffraction analysis (CIF files CCDC no. 1480230) and further characterized by elemental analyses, IR spectra, and thermogravimetric analysis. MOF **I** exhibits a rare (3,4)-connected 2D structure bearing two kinds of organic ligands. According to the crystal data, the coordination ability and mode of the imidazole multi-carboxylate ligand are discussed. Furthermore, the thermal stability and solid-state photoluminescent properties of MOF **I** have been investigated.

Keywords: Cd(II) MOF, imidazole multi-carboxylate, single-crystal X-ray diffraction, the thermal stability and photoluminescent properties

DOI: 10.1134/S1070328420040089

ITRODUCTION

Metal–organic frameworks (MOFs) as new types of crystalline solid materials are an important class of functional materials [1]. Due to their intriguing structural features and outstanding functional advantages, nowadays MOFs present attractive prospects in the fields of catalysis [2], environment protection [3], gas separation [4], drug delivery [5], proton conduction [6–10], and electrochemical sensing [11–13]. However, researchers still need to carefully design and construct more and more MOFs to study their interesting properties and applications.

In this context, to construct various crystalline structures of MOFs with desired properties, designing and choosing the promising organic ligands are very essential. Recently, imidazole-4,5-dicarboxylic acid (H_3IDC) and its derivatives as bridging ligands have attracted much attention [14–18]. To now, a large number of MOFs based on above organic ligands have been described owing to their strong coordination abilities and versatile bridging modes. However, the MOFs bearing aromatic groups modified imidazole dicarboxylate ligands are limited, especially the MOFs constructed by 2-(3-carboxylphenyl)-1*H*-imidazole-4,5-dicarboxylic acid (*m*-$CPhH_4IDC$). To the best of our knowledge, only several examples of the MOFs from *m*-$CPhH_4IDC$ can be found in the reference [19, 20]. For example, the syntheses, crystal structures, thermal and luminescent properties of three MOFs from *m*-$CPhH_4IDC$, namely $[Sr_3(m\text{-}CPhHIDC)_2(H_2O)_3]_n$, $\{[Cd_3(m\text{-}CPhHIDC)_2(H_2O)_8] \cdot 2H_2O\}_n$ in [19] and $[Mn_3(m\text{-}CPhHIDC)_2(Phen)_2]_n$ (Phen = 1,10-phenanthroline) [20], have been reported. These complexes show various structures from two-dimensional layer to three-dimensional architecture. It is noted that the *m*-$CPhH_4IDC$ ligand in these MOFs indicate strong coordination ability. Compared with H_3IDC, *m*-$CPhH_4IDC$ is a promising candidate for building more interesting MOFs owing to its unique bulky aromatic carboxylate groups. Meanwhile, additional carboxylate groups can easily generate metal-rich clusters with other carboxylate groups by the coordination bonds between donor atoms and metal centers.

On the other hand, in general, after imidazole derivatives are coordinated with d^{10} metals, the resulting complexes often show bright ligand-centered luminescence [21–26]. The cadmium ions, in particular, because of their full shell electron structure and suitable size, often form unusual molecular structures after coordination with imidazole-based ligands indicating strong luminescence properties [27, 28].

Prompted by the above considerations, herein, we continue to choose *m*-$CPhH_4IDC$ as an useful bridging ligands to react with Cd^{2+} ion in the presence of one coligand, 2,2'-bipyridine (2,2'-Bipy), to obtain

one novel 2D MOF, $\{[Cd_6(m\text{-CPhHIDC})_4(2,2'\text{-Bipy})_6] \cdot 4H_2O\}_n$ (**I**) (Scheme 1). Its crystal structure, thermal and solid-state photoluminescence properties have also been investigated.

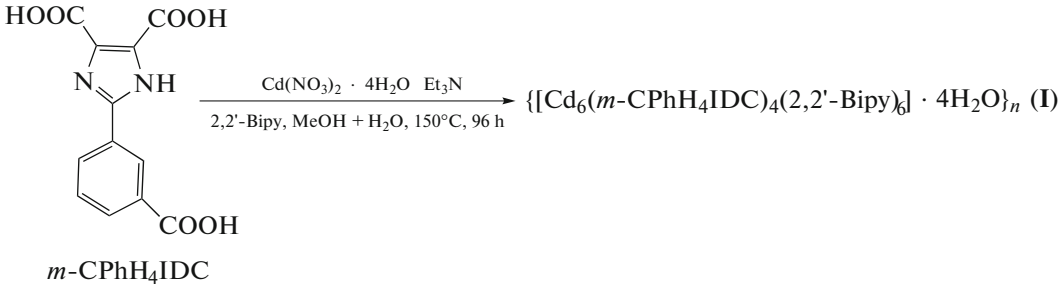

m-$CPhH_4IDC$

Scheme 1.

EXPERIMENTAL

Materials and methods. All chemicals were of reagent grade quality obtained from commercial sources and used without further purification. The organic ligand *m*-$CPhH_4IDC$ was prepared according to the literature procedure [29]. The C, H, and N microanalyses were carried out on a FLASH EA 1112 analyzer. IR spectra were recorded on a Nicolet NEXUS 470-FTIR spectrophotometer as KBr pellets in the 400–4000 cm^{-1} region. Thermal gravimetric (TG) measurements were performed by heating the crystalline sample from 20 to 800°C at a rate of 10°C min^{-1} in air on a Netzsch STA 409PC differential thermal analyzer. Powder X-ray diffraction (PXRD) patterns were collected on Rigaku D/MAX-3 with CuK_α ($\lambda = 1.5418$ Å) irradiation. Fluorescence spectra were characterized at room temperature by a F-4500 fluorescence spectrophotometer.

Synthesis of I. A mixture of $Cd(NO_3)_2 \cdot 4H_2O$ (15.4 mg, 0.1 mmol), *m*-$CPhH_4IDC$ (27.6 mg, 0.1 mmol), 2,2'-Bipy (19.8 mg, 0.1 mmol), CH_3OH–H_2O (3 : 4, 7 mL) and Et_3N (0.084 mL, 0.6 mmol) was sealed in a 25 mL Teflon-lined bomb and heated at 150°C for 96 h and then cooled to room temperature. The colorless cubic crystals of **I** were isolated, washed with distilled water, and dried in air (57% yield based on Cd).

For $C_{108}H_{76}N_{20}O_{28}Cd_6$			
Anal. calcd., %	C, 46.68	H, 2.74	N, 10.09
Found, %	C, 46.79	H, 2.51	N, 10.35

IR (KBr; ν, cm^{-1}): 3418 s, 3066 w, 2928 w, 1678 w, 1616 w, 1472 w, 1381 m, 1262 s, 1117 m, 934 w, 848 s, 787 s, 727 s, 659 w, 639 w, 549 m.

X-ray crystallography. Suitable single crystal was carefully selected under an optical microscope and single-crystal X-ray diffraction data for **I** was recorded on a Bruker smart APEXII CCD diffractometer with a graphite-monochromated MoK_α radiation (λ = 0.71073 Å) at temperature 296.15 K. All data were collected at room temperature using the ω–2θ scan technique and corrected for Lorenz-polarization effects. Furthermore, a correction for secondary extinction was applied. The structure of **I** was solved with the direct methods and expanded using the Fourier technique. The non-hydrogen atoms were refined with anisotropic thermal parameters. Hydrogen atoms were included but not refined. The final cycle of full-matrix least squares refinement was based on 22750 observed reflections and 1489 variable parameters. All calculations were performed using the SHELX-97 crystallographic software package [30]. To refine the crystal data, SQUEEZE procedure was used. The empirical absorption corrections by SADABS were carried out [31]. The crystallographic data, and selected bond lengths and angles of **I** are given in Tables 1 and 2, respectively.

Supplementary material for structure **I** has been deposited with the Cambridge Crystallographic Data Centre (CCDC no. 1480230; deposit@ccdc.cam.ac.uk or https://www.ccdc.cam.ac.uk/deposit).

RESULTS AND DISCUSSION

In MOF **I**, three hydrogen atoms of one imidazole-H, one imidazole COO-H and one phenyl COO-H are triply deprotonated to form the *m*-$CPhHIDC^{3-}$ anion. The discoveries further demonstrate that *m*-$CPhH_4IDC$ has the ability to afford more complicated coordinated modes to meet the requirements of the central metal ion coordination. Being good linkers in tuning construction of MOFs with novel frameworks, the N-donor auxiliary ligands also have significant effects on structure construction and potential properties of MOFs [32–34]. In compound **I**, we introduced 2,2'-Bipy, which is a highly chelating N-containing coligand, into our metal–carboxylate reaction system. Thus, sheet-like complex **I** was obtained. Furthermore, the π–π stacking interactions

between the auxiliary ligands facilitate the formation of 3D supramolecular structure networks. It seems that the large steric hindrance of 2,2'-Bipy ligand gives rise to the reduction of the dimensionality of the structures, which has been reported in previous literatures [35–38].

Complex **I** shows a 2D sheet structure. As shown in Fig. 1a, the asymmetric unit of **I** consists of six crystallographically independent Cd^{2+} ions, four *m*-CPhHIDC^{3-} and six 2,2'-Bipy ligands and four guest water molecules. The Cd(1) atom is surrounded by two nitrogen atoms and two carboxylate oxygen atoms from two individual *m*-CPhHIDC^{3-} ligands, and two nitrogen atoms from a chelating 2,2'-Bipy ligand. The surrounding of atom Cd(2) is similar to that of Cd(1). The Cd(3) shows a six-coordinated coordination environment with one nitrogen atom (N(16)), three carboxylate oxygen atoms (O(1), O(2), and O(13)) from two individual *m*-CPhHIDC^{3-} anions, and two nitrogen atoms (N(1) and N(2)) from 2,2'-Bipy to generate a octahedron geometry [CdO_3N_3]. The surroundings of atoms Cd(4), Cd(5), and Cd(6) are similar to that of Cd(3). The Cd–O and Cd–N bonds lengths are varying from 2.253(8) to 2.354(9) Å and 2.298(7) to 2.449(8) Å, respectively. The bond angles around the central Cd^{2+} ion range from 54.1(3)°–116.5(3)° (cis) and 150.1(4)°–174.6(4)° (trans) (see Table 2), all of which are comparable to those reported for other imidazole-based dicarboxyate Cd(II) complexes [39–42].

Each *m*-CPhHIDC^{3-} unit in **I** adopts only one kind of coordination mode, μ_3-*k*N,O:*k*O',N':*k*O'',*k*O''' (Fig. 2). Two *m*-CPhHIDC^{3-} ligands hold two cadmium atoms together leading to a dinuclear unit. The intradinuclear shortest Cd···Cd distance is 6.7046 Å. Such neighboring units are bridged by μ_3-*m*-CPhHIDC^{3-} ligands into a 1D chain along *b* axis (Fig. 1b). Furthermore, the μ_3-*m*-CPhHIDC^{3-} units in *N*,*O*-chelating fashion bridge these 1D chains to form a 2D network (Fig. 1c).

The IR spectrum of **I** displays characteristic absorption bands for water molecules, carboxylate, imidazole, and phenyl units. The compound **I** shows strong and broad absorption bands in the range of 3400–3500 cm^{-1}, which indicates the presence of the ν(N–H) and the ν(O–H) stretching frequencies of the imidazole ring and coordinated water molecules, respectively. The carboxyl can be observed from the absorption bands in the frequency range 1313–1702 cm^{-1} as a result of $\nu_{as}(COO^-)$ and $\nu_s(COO^-)$ vibrations, respectively. The characteristic IR band of the phenyl ring at 634–860 cm^{-1} is due to δ(CH) vibrations, which can be found at 735, 765, and 849 cm^{-1}. In conclusion, the infrared spectral data of **I** are consistent with crystal structure analysis.

As indicated in Fig. 3, the PXRD spectrum of bulk crystalline samples for **I** is consistent well with the simulated patterns from single crystal data, which indicate the phase purity of **I**.

Table 1. Crystallographic data and structure refinement for complexes **I**

Parameter	Value
Fw	2780.32
Crystal system	Monoclinic
Space group	$P2_1/c$
Crystal size	0.18 × 0.14 × 0.12
a, Å	36.0422(4)
b, Å	12.78120(10)
c, Å	28.5787(3)
β, deg	100.534(4)
V, Å^3	12943.3(2)
Z	4
ρ_{calcd}, mg m^{-3}	1.427
F(000)	5520
θ Range for data collection, deg	1.149–25.000
Index ranges, *h*, *k*, *l*	$-42 \le h \le 40$, $-15 \le k \le 14$, $-33 \le l \le 27$
μ, mm^{-1}	1.041
Reflections collected/ unique (R_{int})	64196/22750 (0.0706)
Reflections with $I > 2\sigma(I)$	11041
Data/restraints/parameters	22750/0/1489
Goodness-of-fit on F^2	1.051
Final *R* indices ($I > 2\sigma(I)$)	$R_1 = 0.0810$, $wR_2 = 0.2088$
R indices (all data)	$R_1 = 0.1471$, $wR_2 = 0.2348$
Largest diff. peak and hole, e Å^{-3}	0.694 and –0.587

To investigate the thermal stability of **I**, we performed TG analysis. The TG curve is provided in Fig. 4, which indicates that **I** shows the first weight loss 36.66% in the temperature range of 45–383°C corresponded to the release of four lattice water molecules and six 2,2'-Bipy units (calced. 36.31%). Then a rapid thermolysis process from 383 to 490°C was in accordance with the decomposition of the four *m*-CPhHIDC^{3-} ligands by a weight loss of 35.43%

Table 2. Selected bond distances (Å) and angles (deg) for complex **I***

Bond	*d*, Å	Bond	*d*, Å	Bond	*d*, Å
N(7)–Cd(1)	2.296(8)	N(10)–Cd(1)	2.257(8)	N(19)–Cd(1)	2.334(9)
N(20)–Cd(1)	2.282(10)	O(10)–Cd(1)	2.431(7)	O(5)–Cd(1)	2.430(7)
N(3)–Cd(2)	2.337(9)	N(4)–Cd(2)	2.318(8)	N(11)–Cd(2)	2.254(8)
N(12)–Cd(2)	2.276(8)	O(15)–Cd(2)	2.440(8)	O(20)–Cd(2)	2.449(8)
N(1)–Cd(3)	2.334(9)	N(2)–Cd(3)	2.341(9)	N(16)–Cd(3)	2.265(8)
O(1)–Cd(3)	2.332(7)	O(2)–Cd(3)	2.369(7)	O(13)–Cd(3)	2.298(7)
N(5)–Cd(4)	2.348(8)	N(6)–Cd(4)	2.354(9)	N(8)–Cd(4)	2.257(8)
O(3)–Cd(4)	2.323(8)	O(11)–Cd(4)	2.352(7)	O(12)–Cd(4)	2.356(7)
O(17)–Cd(5)	2.327(8)	O(23)–Cd(5)$^{\#1}$	2.337(7)	O(24)–Cd(5)$^{\#1}$	2.348(9)
N(13)–Cd(5)	2.253(8)	N(14)–Cd(5)	2.310(10)	N(15)–Cd(5)	2.312(9)
N(9)–Cd(6)	2.302(8)	N(17)–Cd(6)	2.318(10)	N(18)–Cd(6)	2.348(10)
O(7)–Cd(6)	2.351(8)	O(21)–Cd(6)$^{\#2}$	2.351(8)	O(22)–Cd(6)$^{\#2}$	2.331(7)
Angle	ω, deg	Angle	ω, deg	Angle	ω, deg
N(7)Cd(1)O(5)	71.2(3)	N(7)Cd(1)N(19)	93.9(3)	N(7)Cd(1)O(10)	116.5(3)
N(10)Cd(1)N(7)	93.4(3)	N(10)Cd(1)N(19)	167.1(3)	N(10)Cd(1)N(20)	104.3(3)
N(10)Cd(1)O(5)	109.2(3)	N(10)Cd(1)O(10)	71.5(3)	N(19)Cd(1)O(5)	83.3(3)
N(19)Cd(1)O(10)	95.6(3)	N(20)Cd(1)N(7)	158.3(3)	N(20)Cd(1)N(19)	71.4(4)
N(20)Cd(1)O(5)	90.8(3)	N(20)Cd(1)O(10)	81.6(3)	O(5)Cd(1)O(10)	172.2(3)
N(3)Cd(2)O(15)	91.2(3)	N(3)Cd(2)O(20)	83.3(3)	N(4)Cd(2)N(3)	70.8(3)
N(4)Cd(2)O(15)	83.7(3)	N(4)Cd(2)O(20)	95.8(3)	N(11)Cd(2)N(3)	157.9(3)
N(11)Cd(2)N(4)	93.0(3)	N(11)Cd(2)N(12)	93.9(3)	N(11)Cd(2)O(15)	71.7(3)
N(11)Cd(2)O(20)	114.1(3)	N(12)Cd(2)N(3)	105.2(3)	N(12)Cd(2)N(4)	166.5(3)
N(12)Cd(2)O(15)	109.5(3)	N(12)Cd(2)O(20)	70.8(3)	O(15)Cd(2)O(20)	174.2(3)
N(1)Cd(3)O(2)	100.2(3)	N(1)Cd(3)N(2)	71.0(4)	N(2)Cd(3)O(2)	88.7(3)
N(16)Cd(3)N(1)	92.6(4)	N(16)Cd(3)N(2)	161.1(4)	N(16)Cd(3)O(1)	109.6(4)
N(16)Cd(3)O(2)	104.3(3)	N(2)Cd(3)O(13)	100.4(4)	O(1)Cd(3)N(1)	150.1(4)
O(1)Cd(3)N(2)	89.1(4)	O(1)Cd(3)O(2)	55.9(3)	O(13)Cd(3)N(1)	106.7(3)
O(13)Cd(3)N(16)	74.7(3)	O(13)Cd(3)O(1)	98.6(3)	O(13)Cd(3)O(2)	153.1 (3)
N(8)Cd(4)O(12)	102.9(3)	O(3)Cd(4)O(12)	152.9(3)	O(11)Cd(4)N(5)	149.8(4)
N(8)Cd(4)O(3)	75.2(4)	O(3)Cd(4)O(11)	99.0(3)	O(11)Cd(4)N(6)	88.5(4)
N(8)Cd(4)O(11)	108.8(4)	O(3)Cd(4)N(5)	106.6(4)	N(5)Cd(4)O(12)	100.5(4)
N(8)Cd(4)N(5)	93.2(4)	O(3)Cd(4)N(6)	101.1(4)	N(5)Cd(4)N(6)	71.3(4)
N(8)Cd(4)N(6)	162.6(4)	O(11)Cd(4)O(12)	55.4(3)	N(6)Cd(4)O(12)	88.1(3)
N(13)Cd(5)O(17)	73.7(3)	N(14)Cd(5)O(17)	101.1(4)	O(23)$^{\#1}$Cd(5) N(14)	114.7(4)
N(13)Cd(5)N(14)	92.6(4)	N(15)Cd(5)O(17)	95.7(4)	O(23)$^{\#1}$Cd(5)O(17)	144.2(4)
N(13)Cd(5)N(15)	158.5(4)	N(15)Cd(5)N(14)	70.8(5)	O(24)$^{\#1}$Cd(5) O(17)	92.0(4)
N(13)Cd(5)O(23)$^{\#1}$	104.0 (3)	N(15)Cd(5)O(23)$^{\#1}$	95.6(4)	O(24)$^{\#1}$Cd(5) N(14)	157.5(4)
N(13)Cd(5)O(24)$^{\#1}$	108.7(4)	N(15)Cd(5)O(24)$^{\#1}$	89.9(5)	O(24)$^{\#1}$Cd(5)O(23)$^{\#1}$	54.1(3)
N(9)Cd(6)O(7)	74.9(4)	N(9)Cd(6)N(17)	95.7(4)	O(22)$^{\#2}$Cd(6)O(21)$^{\#2}$	56.0(3)
N(9)Cd(6)O(22)$^{\#2}$	105.3(3)	O(7)Cd(6)N(18)	93.4(4)	O(22)$^{\#2}$Cd(6)N(18)	93.1(4)
N(9)Cd(6)O(21)$^{\#2}$	110.1(4)	O(7)Cd(6)N(17)	104.7(4)	O(22)$^{\#2}$Cd(6)N(17)	105.5(4)
N(9)Cd(6)N(18)	159.9(4)	O(22)$^{\#2}$Cd(6)O(7)	149.7(4)	O(21)$^{\#2}$Cd(6)O(7)	94.8(4)
O(21)$^{\#2}$Cd(6)N(17)	151.0(4)	O(21)$^{\#2}$Cd(6)N(18)	86.8(4)	N(17)Cd(6)N(18)	71.1(4)

* Symmetry transformations used to generate equivalent atoms: $^{\#1}$ $-x, y - 1/2, -z + 1/2$; $^{\#2}$ $-x + 1, y + 1/2, -z + 1/2$.

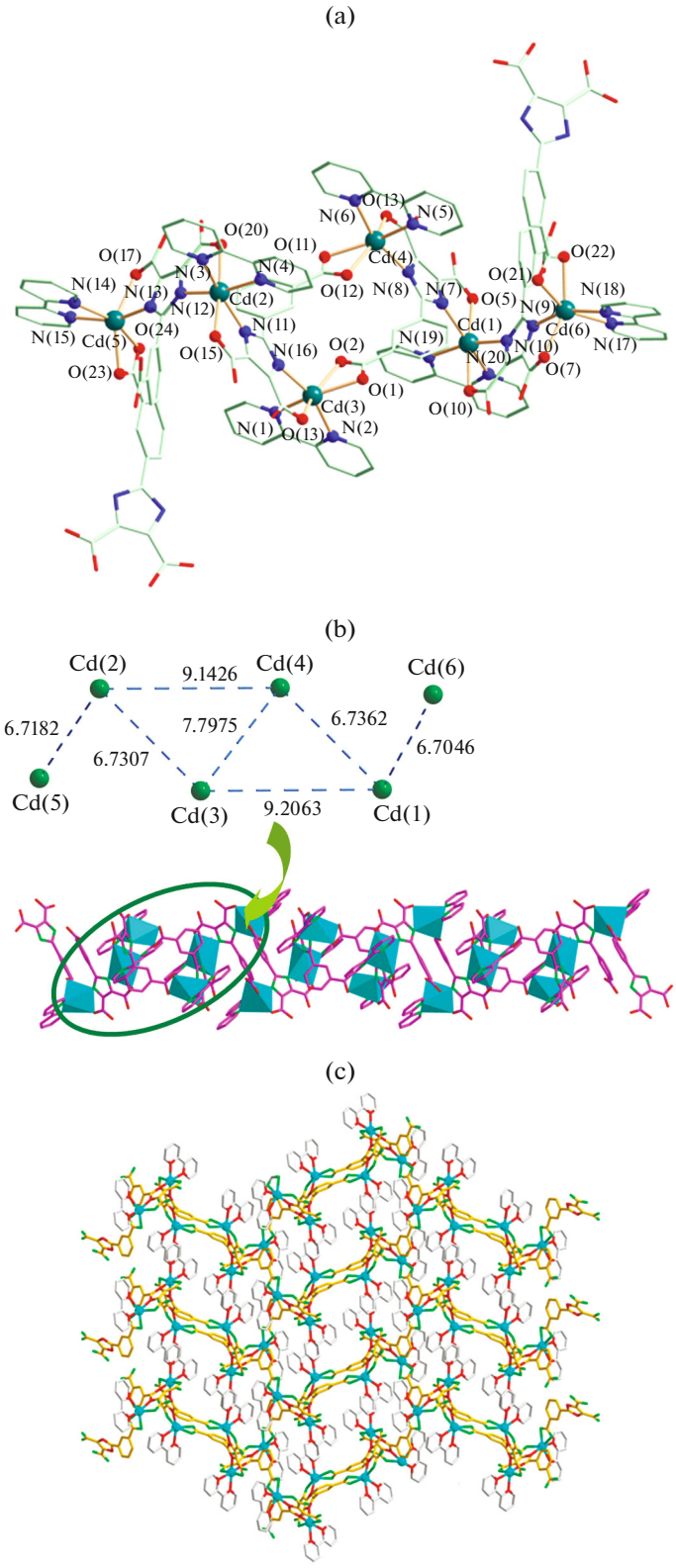

Fig. 1. Coordination environments around the Cd^{2+} ions with atomic lables. H atoms omitted for clarity (a), the 1D wave chain constructed by adjacent interconnected cluster (b), the 2D layer of **I** (c).

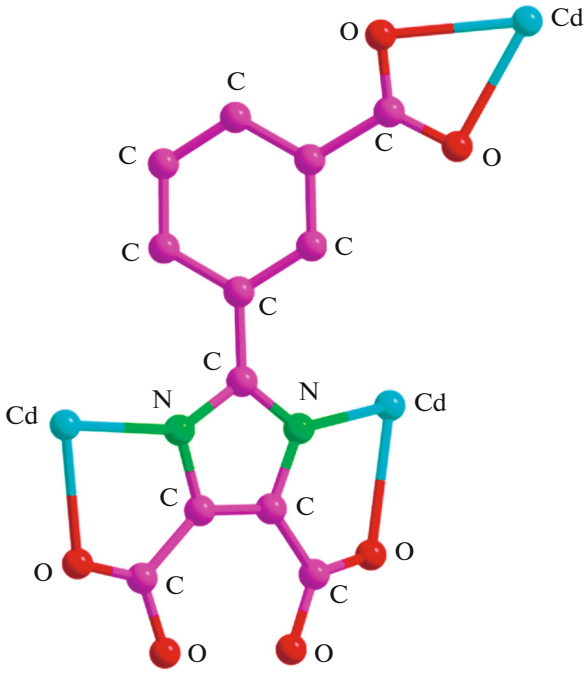

Fig. 2. Coordination mode of *m*-CPhH$_4$IDC ligand in **I**.

(calced. 35.87%). The remaining residue of 27.91% identified to 6CdO (calced. 27.66%).

The photoluminescent behaviors of **I** were investigated in the solid state at room temperature (Fig. 5). As reported in reference [19], the free *m*-CPhH$_4$IDC ligand displays luminescence with the emission maximum at 462 nm by selective excitation at 412 nm,

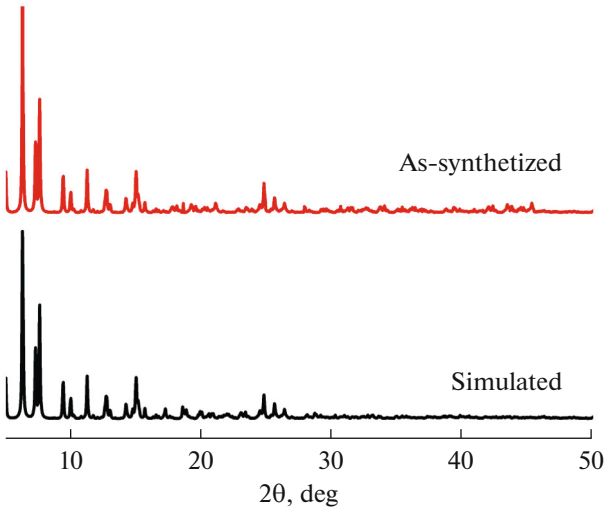

Fig. 3. PXRD patterns of **I** for the simulated and as-synthesized samples.

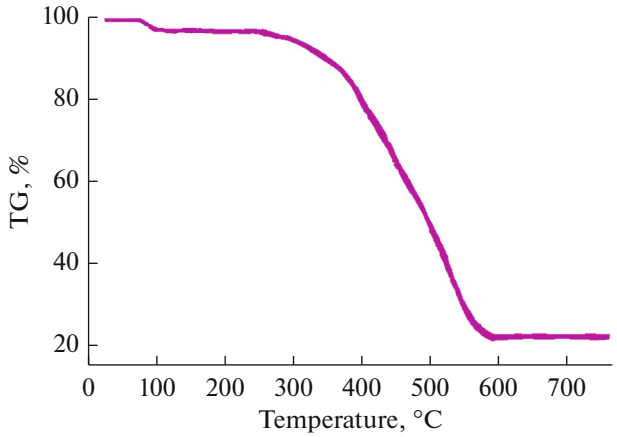

Fig. 4. TG analysis profile of compound **I**.

which may be attributed to ligand-centered $\pi^* \rightarrow n$ or $\pi \rightarrow \pi^*$ electronic transitions. Emission band is observed at 408 nm (λ_{ex} = 355 nm) for **I**. As Cd^{2+} ion with full-shell electronic configuration is difficult to oxidize or reduce, the emission band of MOF **I** cannot be attributed to metal-to-ligand charge transfer (MLCT) or ligand-to-metal charge transfer (LMCT) [42, 43]. The blue shift of compound **I** (54 nm) compared with free *m*-CPhH$_4$IDC ligand may ascribe to a mixture characteristic of intraligand and ligand-to-ligand charge transition (LLCT), as reported for other d^{10} metal complexes with N-donor ligands [44].

FUNDING

We gratefully acknowledge the financial support by Henan Province Education Department Young Key Teachers Project (2016GGJS-265) and Henan Province Education Teaching Reform Research and Practice Project (2017SJGLX658).

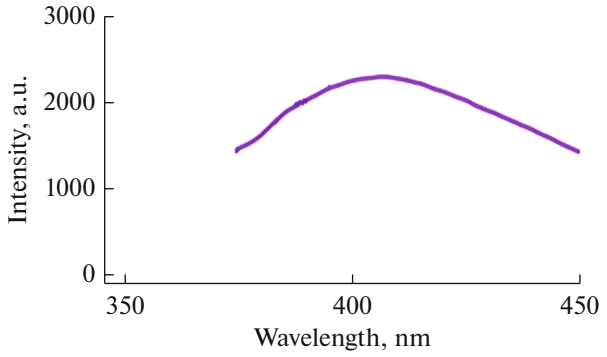

Fig. 5. The solid-state emission spectrum of polymer **I** at room temperature.

REFERENCES

1. Kirchon, A., Feng, L., Drake, H.F., et al., *Chem. Soc. Rev.*, 2018, vol. 47, p. 8611.
2. Wen, Y., Zhang, J., Xu, Q., et al., *Coord. Chem. Rev.*, 2018, vol. 376, p. 248.
3. Dhaka, S., Kumar, R., Deep, A., et al., *Coord. Chem. Rev.*, 2019, vol. 380, p. 330.
4. Zhang, J., Cui, Y., and Qian, G., *Curr. Org. Chem.*, 2018, vol. 22, p. 1792.
5. Isabel, A.L. and Forgan, R.S., *Coord. Chem. Rev.*, 2019, vol. 380, p. 230.
6. Li, A.-L., Gao, Q., Xu, J., et al., *Coord. Chem. Rev.*, 2017, vol. 344, p. 54.
7. Liang, X., Li, B., Wang, M.H., et al., *ACS Appl. Mater. Interfaces*, 2017, vol. 9, p. 25082.
8. Liu, R.L., Zhao, L.L., Dai, W., et al., *Inorg. Chem.*, 2018, vol. 57, p. 1474.
9. Liu, R.L., Zhao, L.L., Yu, S.H., et al., *Inorg. Chem.*, 2018, vol. 57, p. 11560.
10. Chen, W.Y., Zhao, L.J., Yu, S.H., et al., *Polyhedron*, 2018, vol. 148, p. 100.
11. Sun, Z.B., Yu, S.H., Zhao, L.L., et al., *Chem. Eur. J.*, 2018, vol. 24, p. 10829.
12. Guo, K.M., Zhao, L.L., Yu, S.H., et al., *Inorg. Chem.*, 2018, vol. 57, p. 7104.
13. Chen, W.Y., Wang, J., Zhao, L.L., et al., *J. Alloy. Compd.*, 2018, vol. 750, p. 895.
14. Zhang, F.W., Li, Z.F., Ge, T.Z., et al., *Inorg. Chem.*, 2010, vol. 49, p. 3776.
15. Zhong, D.C. and Lu, T.B., *Sci. China-Chem.*, 2011, vol. 54, p. 1395.
16. Wang, W.Y., Yang, Z.L., Wang, C.J., et al., *CrystEngComm*, 2011, vol. 13, p. 4895.
17. Zhang, Y., Luo, X.B., Yang, Z.L., et al., *CrystEngComm*, 2012, vol. 14, p. 7382.
18. Zhang, Y., Guo, B.B., Li, L., et al., *Cryst. Growth Des.*, 2013, vol. 13, p. 367.
19. Guo, B.B., Li, L., Wang, Y., et al., *Dalton Trans.*, 2013, vol. 42, p. 14268.
20. Shi, G.Q., Shi, B.B., Wang, Q., et al., *Polyhedron*, 2015, vol. 92, p. 137.
21. Burlov, A.S., Koshchienko, Y.V., Kiskin, M.A., et al., *J. Mol. Struct.*, 2016, vol. 1104, p. 7.
22. Nikolaevskii, S.A., Koshchienko, Yu.V., Chernyshev, A.V., et al., *Russ. J. Coord. Chem.*, 2014, vol. 40, p. 468. https://doi.org/10.1134/S1070328414070070
23. Koshchienko, Y.V., Burlov, A.S., Makarova, N.I., et al., *Russ. J. Gen. Chem.*, 2017, vol. 87, p. 76. https://doi.org/10.1134/S1070363217010133
24. Burlov, A.S., Koshchienko, Y.V., Makarova, N.I., et al., *Synthetic Met.*, 2016, vol. 220, p. 543.
25. Burlov, A.S., Ikorskii, V.N., Uraev, A.I., et al., *Russ. J. Gen. Chem.*, 2006, vol. 76, p. 1282. https://doi.org/10.1134/S1070363206080214
26. Burlov, A.S., Koshchienko, Y.V., Vlasenko, V.G., et al., *Russ. J. Coord. Chem.*, 2014, vol. 40, p. 531. https://doi.org/10.1134/S1070328414080016
27. Gogoleva, N.V., Shmelev, M.A., Evstifeev, I.S., et al., *Russ. Chem. Bull.*, 2016, vol. 65, p. 181.
28. Nikolaevskii, S.A., Evstifeev, I.S., Kiskin, M.A., et al., *Polyhedron*, 2018, vol. 152, p. 61.
29. Lebedev, A.V., Lebedeva, A.B., Sheludyakov, V.D., et al., *Russ. J. Gen. Chem.*, 2007, vol. 77, p. 949.
30. Sheldrick, G.M., *Acta. Crystallogr., Sect. A: Found. Crystallogr.*, 2008, vol. 64, p. 112.
31. Sheldrick, G.M., *SADABS, Program for Empirical Absorption Correction of Area Detector Data*, Göttingen: Univ. of Göttingen, 1996.
32. Yang, F.F., Wang, X.F., Yu, X.Y., et al., *Polyhedron*, 2015, vol. 98, p. 40.
33. Chen, S.S., Chen, Z.H., Fan, J., et al., *Cryst. Growth Des.*, 2012, vol. 12, p. 2315.
34. Senchyk, G.A., Lysenko, A.B., Krautscheid, H., et al., *Inorg. Chem.*, 2013, vol. 52, p. 863.
35. Tseng, T.W., Luo, T.T., and Shih, Y.R., *CrystEngComm*, 2015, vol. 17, p. 2847.
36. Wang, H.B., Wu, Y.P., and Xu, G.W., *Russ. J. Coord. Chem.*, 2015, vol. 41, p. 664. https://doi.org/10.1134/S107032841510009726
37. Marino, N., Ikotun, O.F., and Julve, M., *Inorg. Chem.*, 2011, vol. 50, p. 378.
38. Fang, S.M., Zhang, Q., and Hu, M., *Cryst. Growth Des.*, 2010, vol. 10, p. 4773.
39. Yue, Z.F., Chen, Z.N., Yao, M.J., et al., *RSC Adv.*, 2014, vol. 4, p. 33537.
40. Jia, H.L., Li, Y.L., Xiong, Z.F., et al., *Dalton Trans.*, 2014, vol. 43, p. 3704.
41. Guo, M.W., Chen, N., Yue, Z.F., et al., *CrystEngComm*, 2012, vol. 14, p. 4955.
42. Wang, F., Jing, X.M., Zheng, B., et al., *Cryst. Growth Des.*, 2013, vol. 13, p. 3522.
43. Li, T.T., Cai, S.L., Zeng, R.H., et al., *Inorg. Chem. Commun.*, 2014, vol. 48, p. 40.
44. Xie, X.X., Zhao, L.L., Liu, Y.X., et al., *New J. Chem.*, 2018, vol. 42, p. 20197.